Solid Earth
Discussions

Open Access

Microscale strain partitioning? Differential quartz lattice preferred orientation development in micaceous phyllite, Hindu Kush, northwestern Pakistan

K. P. Larson[1], J. L. Lamming[2,1], and S. Faisal[1]

[1]Earth and Environmental Sciences, University of British Columbia, Okanagan, 3247 University Way, Kelowna, BC, V1V 1V7, Canada
[2]Department of Geological Sciences, University of Saskatchewan, 114 Science Place, Saskatoon, SK, S7N 5E2, Canada

Correspondence to: K. P. Larson (kyle.larson@ubc.ca)

SED

6, 2735–2758, 2014

Differential quartz lattice preferred orientation development

K. P. Larson et al.

Title Page

Abstract	Introduction
Conclusions	References
Tables	Figures

|◄ ►|

◄ ►

Back Close

Full Screen / Esc

Printer-friendly Version

Interactive Discussion

Abstract

Spatially referenced quartz c axis fabrics demonstrate the preservation of multiple, distinct fabrics in a specimen collected from northwestern Pakistan. The overall fabric yielded by the specimen is dominated by a single population of quartz grains, while the fabric signatures of two other unique, spatially distinct populations are overwhelmed. It is these minor fabrics, however, that provide information on temperature of deformation ($403 \pm 50\,^\circ$C), differential stress ($8.6 + 2.6/-1.5$ MPa to $15.0 + 3.8/-2.5$ MPa), strain rate ($10^{-16}\,\mathrm{s}^{-1}$ to $10^{-15}\,\mathrm{s}^{-1}$), and strain partitioning recorded by the specimen. This work highlights the potential importance of using spatially referenced data when conducting lattice preferred orientation analyses.

1 Introduction

Lattice preferred orientation (LPO) analysis has been long employed to study the strain histories recorded by rock forming minerals (e.g. Turner, 1942; Bouchez and Pêcher, 1976; Lister, 1977; Zhang and Karato, 1995). While investigation of LPOs have been successfully carried out on a wide variety of mineral phases, quartz has been one of the most common targets to elucidate strain within continental crust due to its near ubiquity in such rocks. The development of LPOs in quartz has been actively investigated (e.g Lister and Williams, 1979; Schmid and Casey, 1986), modelled (e.g. Lister, 1977; Lister et al., 1978; Lister and Hobbs, 1980; Keller and Stipp, 2011), and utilized in studies of geologic material (e.g. Bouchez and Pêcher, 1976; Blumenfeld et al., 1986; Law et al., 1990, 2004, 2011, 2013; Xypolias and Koukouvelas, 2001; Larson and Cottle, 2014) during the past five decades. While advances in our understanding and implications of the fabrics have advanced, so too have the methods available to extract lattice orientation data. Universal stages are still employed to generate quartz c axis LPOs, however, more technical methods such as x-ray goniometry and electron backscattered diffraction (EBSD) can potentially provide a higher density of informa-

K. P. Larson et al.

tion and orientation data for secondary axes. In addition, techniques utilizing EBSD and automated optical fabric analysers (e.g. Wilson et al., 2007) have the advantage of producing spatially referenced data with the ability to automatically generate achsenverteilungsanalyse (AVA) or axial distribution diagrams (e.g. Sander, 1950). Such a diagram, essentially a map of crystallographic orientation within the specimen analysed, can help facilitate the investigation and comparison of spatially distinct grains, groups of grains, or zones within a specimen. Spatially referenced LPO patterns also allow for the investigation of strain recorded in grains of various sizes, the potential effects of matrix phases, and the spatial positioning of grains adjacent to local features such as porphyroclasts. While modeling of quartz petrofabrics has produced significant advances in our understanding of LPOs and how to interpret them, advances in spatially referenced LPO analyses now allow us to examine how those LPOs may develop spatially in naturally deformed specimens.

One significant application of spatially referenced LPO data is to examine within-specimen fabric orientation heterogeneities. This type of analysis has been employed to distinguish between preferred orientation in new, recrystallized grains vs. relict porphyroclasts (e.g. Law et al., 2010) and to identify variable dissolution in quartz veins (Wilson et al., 2009). Such studies highlight the potentially significant differences in LPOs for distinct grain populations and/or spatially separated areas of a single specimen. If such careful studies are representative rather than exceptional, the implication is that whole specimen LPO fabrics may represent an averaged fabric in which spatially distinct details, potentially relevant to the strain history of the specimen, are lost or overwhelmed.

This study presents new, spatially referenced LPO data from a specimen collected in the Chitral region of northwestern Pakistan. This specimen records three distinct quartz LPO patterns that can be related to differences in spatial position, recrystallized grain size, and interaction with matrix phases in the specimen. The existence of different LPOs that can be related to significant changes in the texture and/or mineralogy of spatially restricted areas of a specimen may provide insight into strain partitioning at the

microstructural scale. Moreover, the existence of distinct LPOs at the thin section scale has implications for the representation of strain for a specimen using a single LPO and potentially for assessing relative differences between spatially separated specimens.

2 Geological setting

The Chitral region is located within the eastern Hindu Kush of northwestern Pakistan (Fig. 1). The geology of the area is dominated by Paleozoic protoliths, mainly low-grade metasedimentary rocks that locally reach sillimanite grade (Gaetani et al., 1996; Zanchi et al., 2000; Hildebrand et al., 2001; Zanchi and Gaetani, 2011; Faisal et al., 2014). These metasedimentary rocks are intruded by a series of plutonic bodies that range in age from Paleozoic (Kafiristan – 483 ± 21 Ma; Debon et al., 1987), through Mesozoic (Tirich Mir: 114 to 121 Ma, Desio, 1964; Hildebrand et al., 2000; Heuberger et al., 2007 - Buni-Zom: 104 Ma, Heuberger et al., 2007), to Cenozoic (Garam Chasma – 24 Ma; Hildebrand et al., 1998). The region records a protracted deformational history with earliest records indicating Late Triassic deformation and metamorphism and recent events culminating in the Early Miocene (Faisal et al., 2014).

Specimen S32, the subject of the present study, is part of a suite of quartz-rich specimens collected in the Chitral region to investigate the complex deformation history recorded in the area. It is a quartz + muscovite + chlorite phyllite (Fig. 2a, b). The foliation in the specimen is defined by planar muscovite and chlorite laths while the lineation is defined by a grain shape fabric of the same minerals. The specimen has a heterogeneous mineral distribution with localized quartz-rich lenses (Fig. 2a, b) that have a bimodal grain size distribution (Fig. 2d). The coarser population within a large lens has a median area (as calculated for an ellipse using the long and short axes of each grain) in this section of $161\,\mu m^2$ with a standard deviation of 45 and an aspect ratio of 2.5 (standard deviation of 1.0). The smaller grain size population within the same quartz-rich lens is characterized by a median area of $81\,\mu m^2$ with a standard deviation of 20 and an aspect ratio of 2.3 (standard deviation of 1.0). The long axes

Differential quartz lattice preferred orientation development

K. P. Larson et al.

Title Page

Abstract	Introduction
Conclusions	References
Tables	Figures

|◀ | ▶|

◀ | ▶

Back | Close

Full Screen / Esc

Printer-friendly Version

Interactive Discussion

of both grain-size populations are typically at low angles relative to the dominant foliation. The quartz-rich lenses are surrounded by phyllosilicate-rich layers that contain quartz grains with a median elliptical equivalent surface area of 52 μm^2 with a standard deviation of 13 and an aspect ratio of 2.0 (standard deviation of 0.7). These grains are typically elongate parallel to the foliation direction. The LPOs of each quartz grain population are investigated below.

3   Methods

The specimen was geo-oriented during collection and cut parallel to macroscopic lineation and perpendicular to the macroscopic foliation. The orientations of c axes within the specimen were determined using a Russell-Head Designs G50 Automated Fabric Analyser at an optical resolution of 10 μm. Previous research has shown that c axis orientations determined using an automated fabric analyser like the G50 are indistinguishable from those determined using EBSD methods (Wilson et al., 2007; Peternell et al., 2010). The G50 outputs an interactive AVA diagram (Fig. 2c), or c axis map, of the thin section that was used to build LPO patterns. Because each pixel of the AVA diagram has unique c axis orientation data associated with it, the LPO patterns of spatially distinct sections within the specimens can be investigated by picking the exact points/locations/grains from which the orientation data are to be extracted.

The existence of three spatially and texturally distinct quartz grain-size populations within the specimen allows the direct investigation of potential microscale quartz LPO and strain differences. Such investigations allow assessment of the sense of shear recorded by the different populations and the slip systems active during fabric formation. Moreover, the different grain-size populations lend themselves to paleopiezometric investigation through the application of the Stipp and Tullis (2003) paleopiezometer as modified by Holyoke and Kronenberg (2010). These paleopiezometric estimates, in turn, can be combined with derived deformation temperatures to estimate strain rates. The results from this study have bearing on microscale strain, stress, and strain rate

partitioning during deformation and on the potential homogenizing effects of dominant grain size populations in LPO fabric data, which may obscure contributions from other smaller populations.

4 Quartz microstructures and LPOs

The thin section of specimen S32 was cut parallel to the macroscopic lineation ($25° \rightarrow 006°$) and perpendicular to the foliation ($330° / 38°$ NE). In the equal area stereonets used to present the c axis data the lineation lies horizontally across the equator while the foliation is a vertical plane cutting through the equator. The stereonets are oriented such that a dextral asymmetry indicates top-to-the east-southeast shear.

4.1 Quartz textures

The quartz grains that comprise the finer and coarser populations within the quartz-rich lens in the specimen demonstrate textural characteristics consistent with dynamic recrystallization. In both populations there is evidence of minor bulging (Fig. 3a), subgrain development (Fig. 3b, c), and deformation lamellae (Fig. 3b, c). These textures are most consistent with Regime 2 crystallization of Hirth and Tullis (1992) or the SGR category of Stipp et al. (2002).

In contrast, strong evidence for dynamic recrystallization was not observed in the quartz grains found within the phyllitic matrix outside of the quartz-rich lens. Here, the grains are commonly partially surrounded by muscovite and/or chlorite laths (Fig. 3d) and as such typically have restricted contact with one another.

4.2 Quartz LPO fabric results

When examined in bulk (i.e. looking at the fabric automatically generated from a non-discriminant sampling grid) specimen S32 yields a LPO fabric consistent with activation of the basal ⟨a⟩, prism ⟨a⟩, and prism [c] slip systems (Schmid and Casey, 1986;

Differential quartz lattice preferred orientation development

K. P. Larson et al.

Title Page

Abstract | Introduction

Conclusions | References

Tables | Figures

◀◀ | ▶▶

◀ | ▶

Back | Close

Full Screen / Esc

Printer-friendly Version

Interactive Discussion

Fig. 4a). There is a slight asymmetry in the basal ⟨a⟩ fabric that is consistent with top-to-the east-southeast shear. If the LPOs of the three different sized quartz grain populations are examined individually, however, it becomes apparent that the overall, or bulk LPO pattern is dominated by the more abundant matrix quartz population. The

5   LPO fabric yielded from the matrix quartz bears a strong resemblance to the bulk fabric (Fig. 4b). The c axis fabric is slightly different, however, with apparent activation of the rhomb ⟨a⟩ slip system dominant over basal ⟨a⟩ in addition to similar activation of the prism ⟨a⟩ and prism [c] slip systems. Moreover, in the hand-picked pattern there appears to be a stronger prism ⟨a⟩ component and a more well-defined rhomb ⟨a⟩

10   asymmetry (top-to-the-east-southeast). The prism [c] positions also appear to define an asymmetry, but it yields the opposite shear sense to that indicated by the basal ⟨a⟩ fabric (Fig. 4b).

In contrast to both the bulk and the matrix grain-size population, the fabric yielded by the finer size population within the quartz lens comprises a single girdle with activation

15   of the prism ⟨a⟩ and rhomb ⟨a⟩ slip systems (Fig. 4c). There is no indication of prism [c] activation. The single girdle is inclined to the right, which is consistent with top-to-the-east-southeast shear.

The LPO fabric from the coarser grain-size population in the lens is similar to that from the finer-sized population; activation of the prism ⟨a⟩ and rhomb ⟨a⟩ slip systems

20   dominates. Unlike the other intra-lens population, however, the fabric of the coarser-sized grains forms a type-1 crossed-girdle (Fig. 4d). The main fabric displays a top-to-the-right (or southeast) asymmetry, with secondary arms extending away from the main girdle (Fig. 4d).

4.3   Quartz LPO fabric interpretation

25   With the exception of the prism [c] slip (discussed below) the fabric asymmetries noted in the various specimen populations are consistent with the interpreted top-to-the-east/southeast direction of movement across the nearby Tirich Mir fault (Fig. 1; Hildebrand et al., 2001).

Title Page

Abstract | Introduction

Conclusions | References

Tables | Figures

|◀ | ▶|

◀ | ▶

Back | Close

Full Screen / Esc

The overall bulk LPO from the specimen analysed and that of the smaller grain-size population both indicate a component of prism [c] slip. Slip in the prism [c] direction is typically associated with deformation in excess of 600–650 °C (Lister and Dornsiepen, 1982; Mainprice et al., 1986; Morgan and Law, 2004). The rock sampled, however, is a
5 low-metamorphic grade phyllite and has not experienced temperatures in the range of those expected to favour prism [c] slip.

Similar unexpected patterns have been noted in low-metamorphic grade slates and phyllites in New Zealand where they are interpreted to reflect mechanical rotation of grains elongate in the c axis direction parallel with the stretching direction (Stallard
10 and Shelly, 1995). Such an interpretation is consistent with the sparse evidence of dynamic recrystallization in the matrix quartz. However, c axis orientations consistent with slip in the rhomb and prism $\langle a \rangle$ directions indicate that there was some dynamic modification of the crystal lattice in response to deformation. As suggested by Stallard and Shelly (1995), physical rotation of the clasts may have occurred preferentially in
15 the matrix grains surrounded by phyllosilicate-rich layers, into which strain was preferentially partitioned. The matrix quartz grains that occur in areas with less abundant phyllosilicate may have accommodated more of the strain directly through dislocation slip resulting in the development of the prism $\langle a \rangle$ and rhomb/basal $\langle a \rangle$ c axis orientations observed in the LPO.

20 The development of quartz c axis maxima parallel to the stretching lineation may alternatively be explained by preferential dissolution of quartz grains with their (0001) planes parallel to the foliation. The dissolution of such grains and reprecipitation and/or concentration of residual grains with c-axes parallel to the foliation has been interpreted to account for similar c axis patterns in low-metamorphic grade rocks in southeastern
25 Brazil (Hippertt, 1994).

The orientations of c axes in grains that comprise the quartz-rich lens in the specimen appear to have been controlled by dynamic recrystallization (Fig. 3a–c) as part of their deformational response to imposed stresses. Because the quartz records evi-

dence of dynamic recrystallization, the LPO patterns measured from it are interpreted to reflect the modification of its crystal lattice orientation in response to deformation.

4.4 Deformation temperature

The LPO pattern from the coarser grains in the quartz lens forms a weakly developed crossed-girdle fabric (Fig. 4d). The opening angles of such fabrics, that is the angle between the arms of the fabric as measured about the perpendicular to the flow plane, have been empirically related to the estimated temperatures at which the fabrics developed (Kruhl, 1998; Morgan and Law, 2004; Law, 2014). Converting a fabric opening angle into a deformation temperature requires a number of assumptions to be made, including temperature being the primary control on critically resolved shear stress, as opposed to strain rate or hydrolytic weakening. See Law (2014) for an in depth review of the considerations in using quartz LPO opening angles as geothermometers. In reflection of the uncertainty in the data used for the empirical calibration and the precision of the opening angle determined, quartz LPO-derived deformation temperatures are quoted at $\pm 50\,^{\circ}$C (Kruhl, 1998).

The crossed girdle fabric in the specimen analysed has an opening angle of $\sim 53\,^{\circ}$ (Fig. 4d), which corresponds to a deformation temperature of $\sim 403 \pm 50\,^{\circ}$C. That temperature estimate is consistent with the interpreted metamorphic grade of the rock and with the observed microstructures dominated by subgrain development with minor bulging. The transition from bulging to subgrain formation processes in the eastern Tonale fault zone of the Italian Alps is associated with temperatures near $400\,^{\circ}$C (Fig. 9 of Stipp et al., 2002). Similar textures from the Himalaya may occur at slightly higher temperature, closer to $450\,^{\circ}$C (Law, 2014). It should be noted, however, that, as with c-axis opening angles, strain rate and hydrolytic weakening can also play an important role in the development of quartz textures (e.g Law, 2014).

4.5 Quartz grain-Size piezometry and strain rate estimates

Recrystallized grain-size piezometry as proposed by Stipp and Tullis (2003) and re-calibrated by Holyoke and Kronenburg (2010) may be used to estimate potential differences in differential flow stresses recorded in different dynamically recrystallized grain-size populations. Experimental calibration of the quartz grain-size piezometer applies to bulging recrystallization mechanisms and extends to a maximum grain-size of $\sim 50\,\mu m$ (Stipp and Tullis, 2003; Stipp et al., 2006). Stipp et al. (2010) suggest that the piezometer may be reasonably applied grains formed through subgrain rotation recrystallization, but would significantly underestimate those developed during grain boundary migration recrystallization. Applying the quartz recrystallization piezometer to the two dynamically recrystallized size populations in the quartz rich lenses yields differential stresses of $8.6 + 2.6/ - 1.5\,MPa$ and $15.0 + 3.8/ - 2.5\,MPa$ for the coarser and finer quartz grain-size populations respectively.

The differential stress estimates determined can be combined with deformation temperature and plotted atop a series of different geologically reasonable strain rates (Fig. 5). As pressure constraints have not been established for the specimen S32, or any relevant nearby locales, the fugacity used in both the Hirth et al. (2001) and Rutter and Brodie (2004) quartz flow law calibrations utilized was estimated using the derived deformation temperature, a thermal gradient of $25\,^\circ C\,km^{-1}$, and an average crustal density of $2.85\,g\,cm^{-3}$. The resulting fugacity, 108 MPa, was calculated as in Pitzer and Sterner (1994). As noted in Law et al. (2013), calculated strain rates are rather insensitive to changes in fugacity; using a thermal gradient of $40\,^\circ C\,km^{-1}$ in fugacity calculations does not result in a significant change in the strain rate estimates for this study. Plotted differential stresses and deformation temperature indicates a faster strain rate for the finer grains/higher differential stress (Fig. 5). The strain rate estimates vary considerably between the two calibrations with only the Hirth et al. (2001) calibration providing estimates that approach those geologically reasonable (Fig. 5).

Full Screen / Esc

5 Discussion

The size variation between the matrix and lens quartz grains in the specimen may reflect primary differences associated with the protolith. The finer sized quartz grains found within the phyllitic matrix are interpreted to represent smaller grains deposited
5 within a silt/mud dominated protolith, while the coarser quartz that occurs within the specimen is interpreted to represent a thin sand lens. Within the lens itself the two grain size populations may reflect further primary differences, secondary modification during deformation, or both. These possibilities are discussed below.

It is possible that the two grain size populations within the lens reflect different strain
10 histories. The quartz within the lens has been subject to dynamic recrystallization during which there would have been potential for the grains to change size and shape. The grain size difference within the lens may reflect development of the finer population where stress was preferentially partitioned resulting in more intense grain size reduction, whereas the courser population, affected by lower stresses, may relfect more
15 limited grain size reduction. Such stress partitioning is consistent with differential stress estimates made based on grain size piezometry that indicated higher stresses associated with smaller grain sizes.

The two grain sizes may, alternatively (or additionally), reflect an initial difference in grain size inherited from the sand lens when it was first deposited, perhaps com-
20 pounded by incomplete recrystallization of the larger grains. The variation in grain size within the quartz-rich lens may represent a combination of both primary differences and secondary strain partitioning. Finer grains within the quartz lens may have been preferred for initial strain partitioning, which would have facilitated, and been enhanced by, further grain size reduction and higher strain rates. Strain concentration within the finer
25 grains in the quartz-rich lens is consistent with the variation in LPO fabrics in the two size populations. The coarser grain size fabric maintains secondary trailing arms (Fig 4d), whereas in the finer grain size fabric those arms have been essentially obliterated (Fig. 4c). Migration towards a single girdle fabric has been associated with increased

critically resolved shear stress (Lister and Paterson, 1979) and shear strain (Keller and Stipp, 2011) in quartz LPO evolution models.

6   Conclusions

This study demonstrates the importance of spatial resolution and registration in speci-
mens analyzed for petrofabric analyses. In this metapelite example, the bulk LPO fabric overwhelmed two spatially restricted fabrics recorded in a quartz lens. Yet it was the secondary, spatially distinct fabrics that yielded information on deformation temper-ature, paleopiezometry, and strain rate. This has important implications for increas-ingly common studies that examine large numbers of specimens utilizing automated methods; care must be taken to investigate the spatial distribution of fabric symmetry within specimens as the bulk pattern may average and mask important information. The spatially-controlled LPO patterns documented in this study may reflect the funda-mental initial properties of the specimen, be products of differential strain partitioning at the microscale, or some combination of the two.

References

Blumenfeld, P., Mainprice, D., and Bouchez, J.-L.: *C*-slip in quartz from subsolidus deformed granite, Tectonophysics, 127, 97–115, 1986.
Bouchez, J.-L. and Pêcher, A.: Plasticite du quartz et sens de cisaillement dans des quartzites du Grand Chevaughement Central himalayen, Bulletin du societie geologique, France, 7, 1377–1385, 1976.

Debon, F., Afzali, H., LeFort, P., and Sonet, J.: Major intrusive stages in Afghanistan: typology, age, and geodynamic setting. Geologische Rundschau, 76, 245–264, 1987.

Desio, A.: On the geological age of some granites of the Karakoram, Hindu Kush and Badakhshan (central Asia), in: Proceeding of the 22nd International Geological Congress, Delhi, Part II, Section 11, 479–496, 1964.

Faisal, S., Larson, K. P., Cottle, J. M., and Lamming, J.: Building the Hindu Kush: Monazite Records of Terrane Accretion, Plutonism, and the Evolution of the Himalaya-Karakoram-Tibet Orogen, Terra Nova, 26, 395–401, doi:10.1111/ter.12112, 2014.

Gaetani, M., Le Fort, P., Tanoli, S., Angiolini, L., Nicora, A., Sciunnach, D., and Asif, K.: Reconnaissance geology in Chitral, Baroghil and Karambar districts (N Pakistan), Geol. Rundsch., 85, 683–704, 1996.

Heuberger, S., Schaltegger, U., Burgi, J.P., RG1, Villa, I.M., Frank, M., Dawood, H., Hussain, S., Zanchi, A.: Age and isotopic constraints on magmatism along the Karakoram-Kohistan Suture Zone, NW Pakistan: evidence for subduction and continued convergence after India-Asia collision, Swiss J. Geosci., 100, 85–107, 2007.

Hildebrand, P. R., Noble, S. R., Searle, M. P., Parrish, R. R., and Shakirullah: Tectonic significance of 24 Ma crustal melting in the eastern Hindu Kush, Pakistan, Geology, 26, 871–874, 1998.

Hildebrand, P. R., Searle, M. P., Shakirullah, Khan, Z., and Van Heijst, H.: Geological evolution of the Hindu Kush, NW Frontier Pakistan: active margin to continent-continent collision zone, Geol. Soc. London, Special Publications, 170, 277–293, 2000.

Hildebrand, P. R., Noble, S. R., Searle, M. P., Waters, D. J., and Parrish, R. R.: Old origin for an active mountain range: Geology and geochronology of the eastern Hindu Kush, Pakistan, Geol. Soc. Am. Bull., 113, 625–639, 2001.

Hippertt, J. F.: Microstructures and c axis fabrics indicative of quartz dissolution in sheared quartzites and phyllonites, Tectonophysics, 229, 141–163, 1994.

Hirth, G. and Tullis, J.: Dislocation creep regimes in quartz aggregates, J. Struct. Geol., 14, 145–160, 1992.

Hirth, G., Teyssier, C., and Dunlap, J.: An evaluation of quartzite flow laws based on comparisons between experimentally and naturally deformed rocks, Int. J. Earth Sci., 90, 77–87, 2001.

Title Page

Abstract | Introduction

Conclusions | References

Tables | Figures

|◀ | ▶|

◀ | ▶

Back | Close

Full Screen / Esc

Printer-friendly Version

Interactive Discussion

Holyoke III, C. W., and Kronenberg, A. K.: Accurate differential stress measurement using the molten salt cell and solid salt assemblies in the Griggs apparatus with applications to strength, piezometers and rheology, Tectonophysics, 494, 17–31, 2010.

Keller, L. M. and Stipp, M.: The single-slip hypothesis revisited: Crystal-preferred orientations of sheared quartz aggregates with increasing strain in nature and numerical simulation, J. Struct. Geol., 33, 1491–1500, 2011.

Kruhl, J. H.: Reply: Prism- and basal plane parallel subgrain boundaries in quartz: a microstructural geothermobarometer, J. Metamor. Geol., 16, 142–146, 1998.

Larson, K. P. and Cottle, J. M.: Midcrustal discontinuities and the assembly of the Himalayan midcrust, Tectonics, 33, 718–740, doi:10.1002/(ISSN)1944-9194, 2014.

Law, R. D.: Deformation thermometry based on quartz c axis fabrics and recrystallization microstructures: A review, J. Struct. Geol., 66, 129–161, 2014.

Law, R. D., Schmid, S., and Wheeler, J.: Simple Shear Deformation and Quartz Crystallographic Fabrics – a Possible Natural Example From the Torridon Area of Nw Scotland, J. Struct. Geol., 12, 29–45, 1990.

Law, R. D., Searle, M. P., and Simpson, R. L.: Strain, deformation temperatures and vorticity of flow at the top of the Greater Himalayan Slab, Everest Massif, Tibet, J. Geol. Soc., 161, 305–320, 2004.

Law, R. D., Mainprice, D., Casey, M., Lloyd, G., Knipe, R., Cook, B., and Thigpen, J.: Moine Thrust zone mylonites at the Stack of Glencoul: I-microstructures, strain and influence of recrystallization on quartz crystal fabric development, Geological Society London Special Publications, 335, 543–577, 2010.

Law, R. D., Jessup, M. J., Searle, M. P., Francsis, M. K., Waters, D. J., and Cottle, J. M.: Telescoping of isotherms beneath the South Tibetan Detachment System, Mount Everest Massif, J. Struct. Geol., 33, 1569–1594, 2011.

Law, R. D., Stahr, D. W., Francsis, M. K., Ashley, K. T., Grasemann, B., and Ahmad, T.: Deformation temperatures and flow vorticities near the base of the Greater Himalayan Series, Sutlej Valley and Shimla Klippe, NW India, J. Struct. Geol., 54, 21–53, 2013.

Lister, G. S.: Crossed-girdle c-axis fabrics in quartzites plastically deformed by plane strain and progressive simple shear, Tectonophysics, 39, 51–54, 1977.

Lister, G. S. and Dornsiepen, U. F.: Fabric transitions in the Saxony granulite terrain, J. Struct. Geol., 4, 81–92, 1982.

Title Page

Abstract | Introduction

Conclusions | References

Tables | Figures

|◀ | ▶|

◀ | ▶
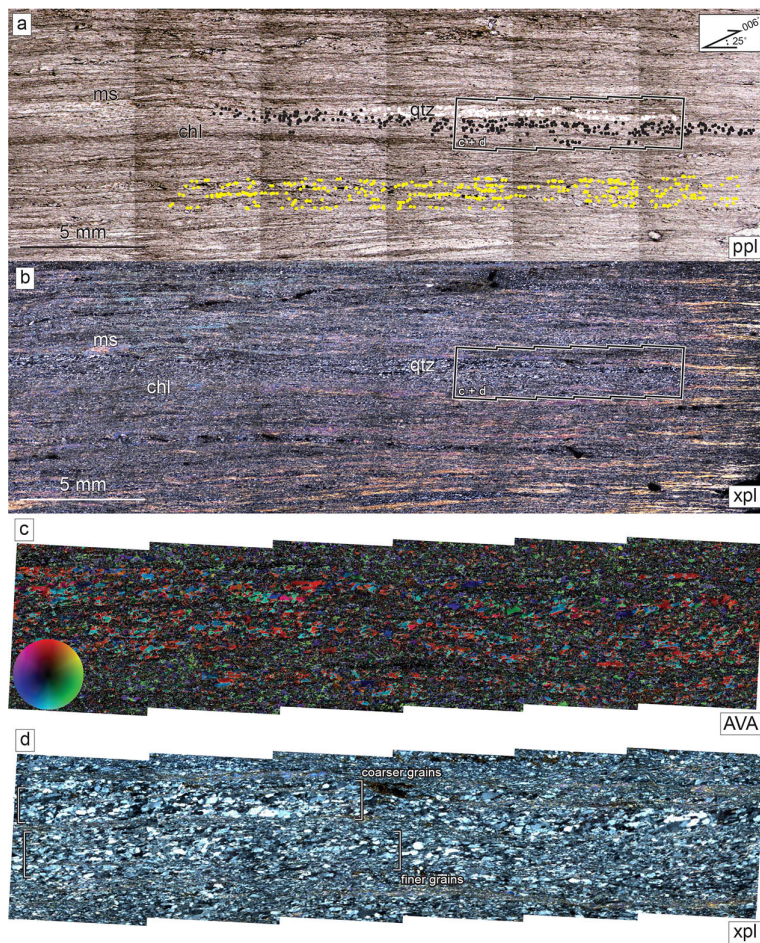
Back | Close

Full Screen / Esc

Printer-friendly Version

Interactive Discussion

Lister, G. S. and Hobbs, B. E.: The simulation of fabric development during plastic deformation and its application to quartzite: the influence of deformation history, J. Struct. Geol., 2, 355–370, 1980.

Lister, G. S. and Paterson, M. S.: Simulation of fabric development during plastic deformation and its application to quartzite fabric transitions, J. Struct. Geol., 1, 99–115, 1979.

Lister, G. S. and Williams, P. F.: Fabric development in shear zones: theoretical controls and observed phenomena, J. Struct. Geol., 1, 283–297, 1979.

Lister, G. S., Paterson, M. S., and Hobbs: Simulation of fabric development in plastic deformation and its application to quartzite – the model, Tectonophysics, 45, 107–158, 1978.

Mainprice, D. Bouchez, J. L., Blumenfeld, P., and Tubia, J. M: Dominant c slip in naturally deformed quartz: implications for dramatic plastic softening at high temperature, Geology, 14, 819–822, 1986.

Morgan, S. S. and Law, R. D.: Unusual transition in quartzite dislocation creep regimes and crystal slip systems in the aureole of the Eureka Valley-Joshua Flat-Beer Creek pluton, California: a case for anhydrous conditions created by decarbonation reactions, Tectonophysics, 384, 209–231, 2004.

Peternell, M., Hasalová, P., Wilson, C. J. L., Piazolo, S. and Schulmann, K.: Evaluating quartz crystallographic preferred orientations and the role of deformation partitioning using EBSD and fabric analyser techniques, J. Struct. Geol., 32, 803–817, 2010.

Pitzer, K. S. and Sterner, S. M.: Equations of state valid continuously from zero to extreme pressures for H_2O and CO_2, J. Chem. Phys., 101, 3111–3116, 1994.

Rutter, E. and Brodie, K.: Experimental intracrystalline plastic flow in hot-pressed synthetic quartzite prepared from Brazilian quartz crystals, J. Struct. Geol., 26, 259–270, 2004.

Schmid, S. M. and Casey, M.: Complete fabric analysis of some commonly observed quartz [c]-axis patterns, in: Mineral and Rock Deformation: Laboratory Studies, edited by: Hobbs, B. E. and Heard, H. C., Geophys. Monogr., 36, 263–286, 1986.

Stallard, A. and Shelly, D.: Quartz c-axes parallel to stretching directions in very low-grade metamorphic rocks, Tectonophysics, 249, 31–40, 1995.

Stipp, M. and Tullis, J.: The recrystallized grain size piezometer for quartz, Geophys. Res. Lett., 30, 2088, doi:10.1029/2003GL018444, 2003.

Stipp, M., Stúnitz, H., Heilbronner, R., and Schmid, S. M.: The eastern Tonale fault zone: a natural laboratory for crystal plastic deformation of quartz over a temperature range from 250 to 700 °C, J. Struct. Geol., 24, 1861–1884, 2002.

Stipp, M., Tullis, J., and Behrens, H.: Effect of water on the dislocation creep microstructure and flow stress of quartz and implications for the recrystallized grain size piezometer, J. Geophys. Res., 111, B042201, doi:10.1029/2005JB003852, 2006.

Stipp, M., Tullis, J., Scherwath, M., and Behrmann, J. H.: A new perspective on paleopiezome-try: Dynamically recrystallized grain size distributions indicate mechanism changes, Geology, 38, 759–762, 2010.

Turner, F. J.: Preferred orientation of olivine crystals in peridotite, Trans. Proc. Roy. Soc. New Zealand, 72, 280–300, 1942

Wilson, C. J. L., Russell-Head, D. S., Kunze and Viola, G.: The analysis of quartz c-axis fabrics using a modified optical microscope, J. Microsc.-Oxford, 227, 30–41, 2007.

Wilson, C. J. L., Robinson, J., and Dugdale, A.: Quartz vein fabrics coupled to elevated fluid pressures in the Stawell gold deposit, south-eastern Australia, Mineralium Deposita, 44, 245–263, 2009.

Xypolias, P. and Koukouvelas, I. K.: Kinematic vorticity and strain rate patterns associated with ductile extrusion in the Chelmos Shear Zone (External Hellenides, Greece), Tectonophysics, 338, 59–77, 2001.

Zanchi, A. and Gaetani, M.: The geology of the Karakoram range, Pakistan: the new 1 : 100 000 geological map of Central-Western Karakoram, Ital. J. Geosci., 130, 161–262, 2011.

Zanchi, A., Poli, S., Fumagalli, P., and Gaetani, M.: Mantle exhumation along the Tirich Mir Fault Zone, NW Pakistan: pre-mid-Cretaceous accretion of the Karakoram terrane to the Asian margin, in: Tectonics of the Nanga Parbat Syntaxis and the Western Himalaya, edited by: Khan, M. A., Treloar, P. J., Searle, M. P., and Jand, M. Q., Geol. Soc. London, Special Publication, 170, 237–252, 2000.

Zhang, S. and Karato, S. I.: Lattice preferred orientation of olivine aggregates deformed in simple shear, Nature, 375, 774–777, 1995.
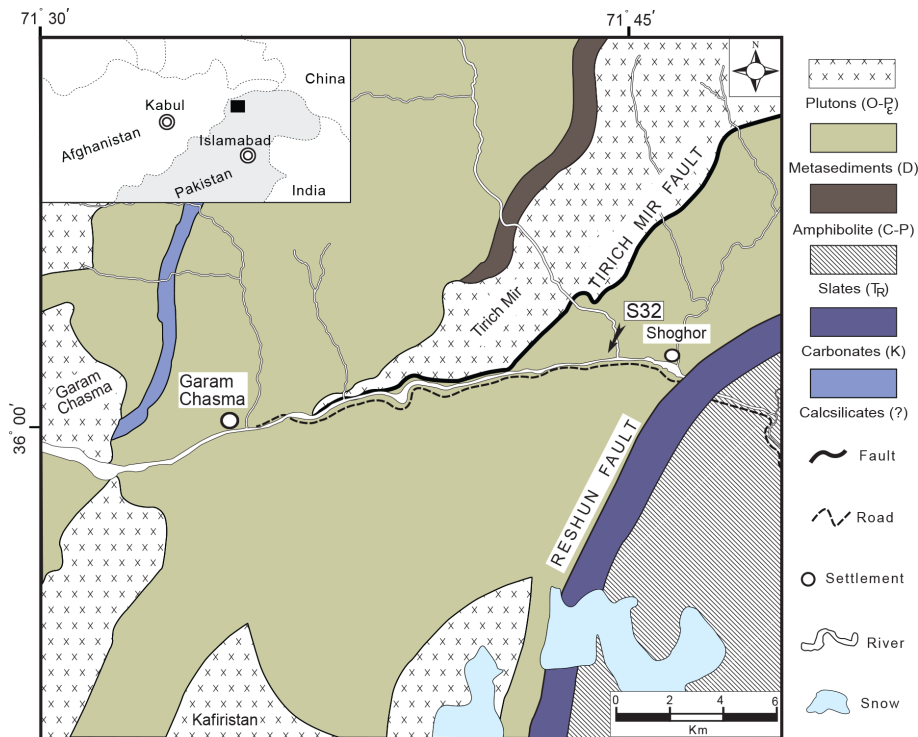
Figure 1. General geology map of the Garam Chasma/Chitral region, NW Pakistan. Geology is after Hildebrand et al. (2000) and Faisal et al. (2014). Specimen collection location is indicated. Field area location is shown in regional scale inset map.

Figure 2. Caption on next page.

Figure 2. Thin section scale photomicrographs of specimen S32 presented in plane-polarized light **(a)** and cross-polarized light **(b)**. The location of quartz grains used for petrofabric analyses is indicated by different coloured and shaded circles in **(a)**. White circles denote a coarser grain within the quartz-rich lens; black circles indicate a finer grain within a quartz-rich lens; yellow circles mark a matrix quartz grain measured. More detailed sections (location shown in **a** and **b**) of the quartz-rich lens are shown in **(c)** as an achsenverteilungsanalyse (AVA) diagram, and in **(d)** as a cross-polarized photomicrograph; coarser and finer populations are marked.
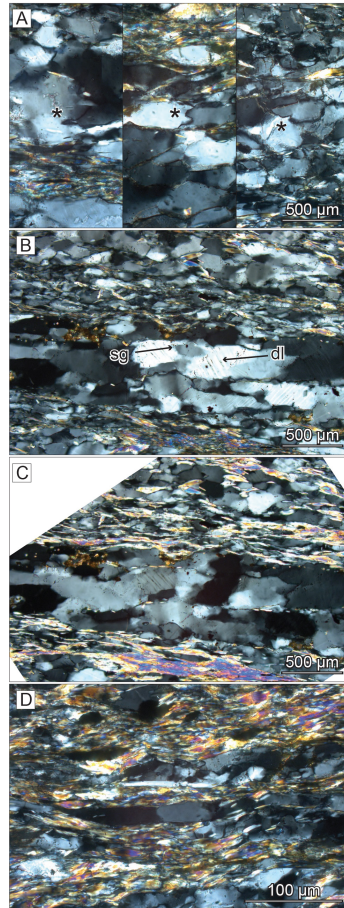
Figure 3. Caption on next page.

Figure 3. Quartz microtextures observed in thin section. All photomicrographs are cross-polarized light. **(a)** Three examples of minor bulging recrystallization (marked). **(b)** Subgrain (sg) development within the quartz- rich lens. Also visible are deformation lamellae (dl). **(c)** Same location as in **(b)** with the stage rotated to further highlight subgrain formation. **(d)** A matrix quartz grain (centre) encased by phyllosilicates.
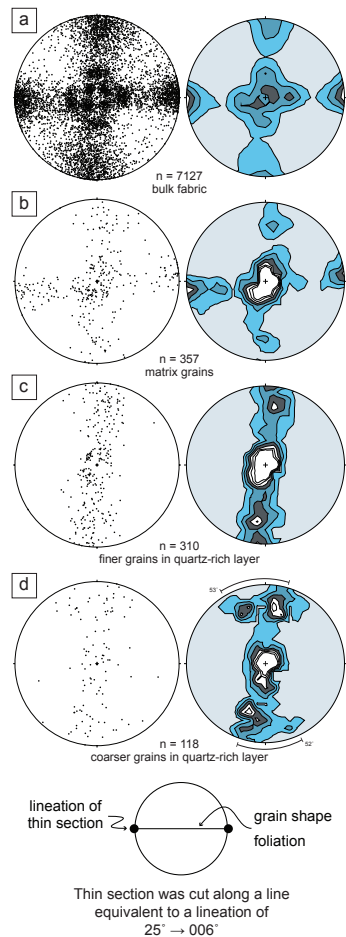
Figure 4. Caption on next page.

Figure 4. Quartz lattice preferred orientation fabrics from various quartz populations in the specimen. All diagrams are lower hemispherical equal area stereonet projections contoured at 1 % intervals. Contours for **(a)** are 1, 2, 3, 4 times uniform; for **(b)** through **(d)** they are 1, 2, 3, 4, 5, 6+ times uniform. The stereonets are oriented such that the foliation forms a vertical plane while the observed lineation (and orientation of thin section) follows a horizontal E-W line. **(a)** Combined/bulk lattice preferred orientation fabric from automated generation across the specimen. **(b)** Quartz lattice preferred orientation fabric generated exclusively from matrix grains. **(c)** Lattice prefered orientation fabric of the finer sized quartz population within the quartz-rich lens. **(d)** Lattice prefered orientation fabric of the coarser sized quartz population within the quartz-rich lens.
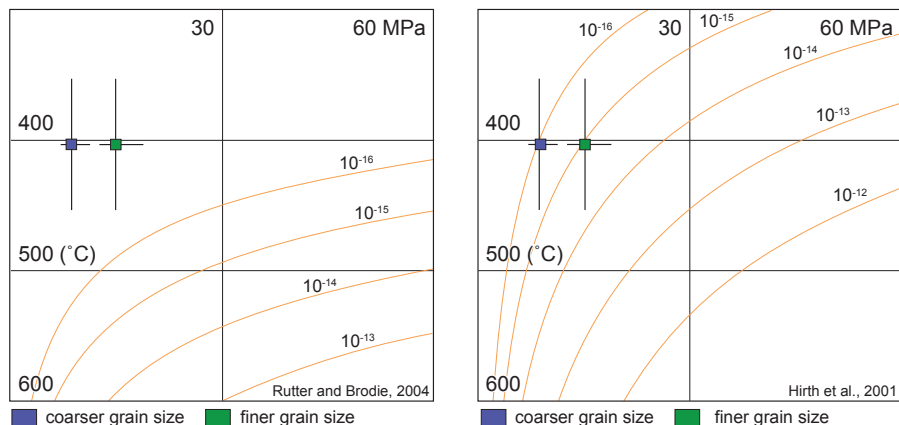
Figure 5. Strain rate estimates for the two size populations within the quartz rich lenses using the flow laws of Hirth et al. (2001) and Rutter and Brodie (2004). Differential stress estimates are from recrystallized grain-size piezometry while temperature estimates are from quartz lattice prefered orientation opening angles. See text for discussion.